Exoplanets Around Red Giants: Distribution and Habitability

Ruixuan Ellie Chen , Jonathan H. Jiang * , Philip E Rosen , Kristen A Fahy , Yanbei Chen

Posted Date: 19 October 2023

doi: 10.20944/preprints202310.1187.v1

Keywords: exoplanet; red giant; habitable zone

Article

Exoplanets Around Red Giants: Distribution and Habitability

Ruixuan E. Chen [1,2], Jonathan H. Jiang [2,*], Philip E. Rosen [3], Kristen A. Fahy [2] and Yanbei Chen [4]

[1] Arcadia High School, Arcadia, CA 91006
[2] Jet Propulsion Laboratory, California Institute of Technology, Pasadena, CA 91099
[3] Independent Researcher, Vancouver, WA 98662
[4] Burke Institute for Theoretical Physics, California Institute of Technology, Pasadena, CA 91125
* Correspondence: Jonathan.H.Jiang@jpl.nasa.gov

Abstract: As the search for exoplanets continues, more are being discovered orbiting Red Giant stars. We use current data from the NASA Exoplanet Archive to investigate planet distribution around Red Giant stars and their presence in the host's habitable zone. As well, we explore the distribution of planet mass and orbital semi major axis for evolved stars with increasing stellar radii. We found 9 Red Giant-hosted exoplanets, and 21 Subgiant-hosted exoplanets to be in the optimistically calculated habitable zone, 5 and 17 of which are in a more conservatively calculated habitable zone. All the planets detected within their habitable zone orbit stars that are in early stages of evolution. We believe that with more powerful instrumentation, more habitable planets may be found around stars that are in later stages of evolution.

Keywords: exoplanet; red giant; habitable zone

1. Introduction

In the distant future when our Sun becomes a Red Giant (RG), the habitable zone (HZ) in the Solar System may move towards the outer planets where the moons of Jupiter and Saturn might be candidates for our future generations to live (Sparrman 2022). Near-term considerations also prompt interest in exoplanet and exomoon systems of RG hosts as some of these worlds may presently be in the HZ of their parent star. In this paper we examine data from the NASA Exoplanet Archive, focusing on exoplanets around Red Giant (or Subgiant) stars.

When a star leaves the Main Sequence (MS) and begins its evolution into the Red Giant Branch (RGB), it undergoes a series of changes. As the fusion of hydrogen progresses in the core of a Main Sequence star, its effective temperature and luminosity increase slowly over time. At the end of a star's Main Sequence stage its core is composed of helium while hydrogen begins to burn in the shell surrounding the core. The star then moves along the RGB of the Hertzsprung-Russell (H-R) diagram, with its temperature moderately decreasing, and its radius and luminosity significantly increasing.

As the host star evolves beyond MS, the orbits of its planets will also evolve. Due to the host's mass loss, its surrounding planets will move outwards (Zahn 1977). On the other hand, tidal interactions tend to shrink the orbital radius of the planets (Villaver et al. 2014). In particular, Villaver et al. 2014 predicted that tidal interaction would cause planets to plunge into the star, and get *engulfed*, before $a/R_s < 3$, where a is the orbital semi-major axis of the planet and R_s is the stellar radius.

The first aim of our paper is to study the distribution of planets around RGs. Previous research (Jiang and Zhu 2018) found a power law relation between planet mass and stellar radius. The associated distribution of three variables is focused upon: the mass of the planet (M_p), the radius of the star (R_s), and the orbital semi-major axis (a). We aim to gain additional insight into the evolution of planets as the host star evolves post-Main Sequence.

To scientists, and the general public alike, habitability and the existence of extraterrestrial life is a topic of high interest (Kaltenegger 2017). A habitable zone is an annular region around a given star where any hosted planets have a relatively high likelihood of moderate average surface temperature, allowing for biological life (as we know it) to possibly exist. The HZ is usually determined primarily

Preprints (www.preprints.org) | NOT PEER-REVIEWED | Posted: 19 October 2023 doi:10.20944/preprints202310.1187.v1

by the stellar energy flux from the host. More specifically, however, for a planet to be habitable it must not only be in its host's HZ, but also possess the appropriate atmospheric and geological conditions accommodative to maintaining surface liquid water.

It has been predicted by many authors that as the Sun enters the RGB, Earth will no longer be in the Solar System's HZ. As investigated by many studies (Danchi et al. 2005, Lopez et al. 2005, Cuntz et al. 2012, Ramirez and Kaltenegger 2016, Gallet et al. 2019, Sparrman 2022), post-MS evolution of the Sun will alter its HZ, possibly rendering some of the outer planets' moons habitable to life such as found on Earth.

For a grid of stars with various mass and metallicity, Ramirez and Kaltenegger (2016) explored the evolution models of planets with their stars, and subsequent durations of planets in the HZ in detail. Their findings suggest three candidate systems that will become habitable once the host star becomes a RG. In this paper we apply the criterion used by two previous studies (Ramirez and Kaltenegger 2016, Sparrman 2022), initially proposed by Kopparapu and colleagues (Kopparapu et al. 2013), to current data in the NASA Exoplanet Archive (NEA), identifying those exoplanets in the HZ and discussing further parameterized regions not yet observed which may also contain habitable planets.

2. Data Collection and Distribution of Planets Around Red Giants

In this section, we briefly introduce our data collection and then discuss the distribution of Sub Giant (SG) and RG planets in the (M_p, a, R_s) parameter space. In Figure 1, we plot an H-R diagram of host stars using luminosity relative to the Sun ($L/L_\odot$) and stellar surface effective temperature (T_{eff}) values from the NEA, identifying 210 RG planets and 229 SG planets, as indicated by red × and blue +, respectively. Parameters of each planet and their host, namely (M_s, R_s, a, M_p) have been listed in Tables A1 and A2 in the Appendix. To estimate the evolutionary stages of each star, we use MIST v1.2 stellar evolution tracks for solar metallicity stars with v/v_{crit}=0.4 (Dotter et al. 2016). In the figure, the purple curve indicates the end of the main sequence, while the separation between SG and RG can be seen from the shapes of the tracks. In this case, we have approximately separated SG and RG using black dashed lines. In comparison with Ghezzi et al. 2010, who used a color-independent M_{bol}=2.82 as the boundary between SG and RGs, our criterion further includes a few more stars, which, according to the evolutionary tracks, are in the RGB despite their relatively low luminosities. We caution that our identification of SG from MS stars can be inaccurate since we have not individually accounted for the metallicity of each host star.

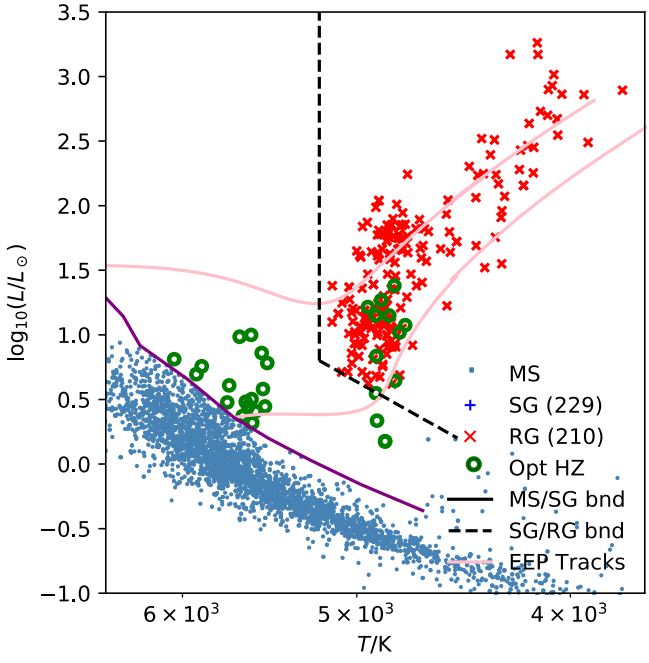

Preprints (www.preprints.org) | NOT PEER-REVIEWED | Posted: 19 October 2023 doi:10.20944/preprints202310.1187.v1

Figure 1. H-R diagram of host stars from the 5063 confirmed planets in the NASA Exoplanet Archive. Separated out are the 210 RG planets and 229 SG planets via the host star's location on the H-R diagram. The purple curve represents the end of the MS, separating SG (blue +) from the MS stars (blue dots). The black dashed line further separates the RGs (red ×) from the SGs (blue +). The pink curves are post-MS evolutionary tracks (EEP tracks) from MIST v1.2 for solar metallicity stars (with $1M_{\odot}$ and $2M_{\odot}$ tracks in solid). Green circles indicate hosts of optimistically habitable planets.

We note that some of these planets, including 42 Dra, γ Dra (Döllinger and Hartmann 2021, henceforth referred to as D&H), and α Tau (Reicher et al. 2019), have been questioned as false positives. D&H further speculated that a substantial fraction of planets around K-giants with radii greater than $21R_{\odot}$ can be false positives, based on the congregation of their orbital periods, lack of planet-metallicity correlation, as well as the excess number of planets around K-giants compared with MS stars. We shall make comparisons with D&H in Section 2.2 below.

2.1. Observed Evolution of Exoplanet Population as the Host Star Evolves

A previous study (Jiang and Zhu 2018) derived a planet mass-stellar radus relation for 150 exoplanets orbiting Red Giants:

$$M_p/M_{\oplus} = a\left(R/R_{\odot}\right)^b \qquad (1)$$

with best-fit parameters a=150 and b=0.88. With the new data points we still see that there is a trend between M_P and R_s, yet their distribution appears to more be in a triangular distribution rather than a linear dependence. Further investigation of the origin of the M_P vs. R_s relation notes that the stellar radius tracks with the post-MS evolution stage of the host star. The fact that M_P increases with R_s corresponds to a relative lack of less massive planets around more evolved stars. In this paper, we shall use Figures 3 and 4, in addition to Figure 2, to further investigate the evolution of the population of exoplanets around stars as they evolve.

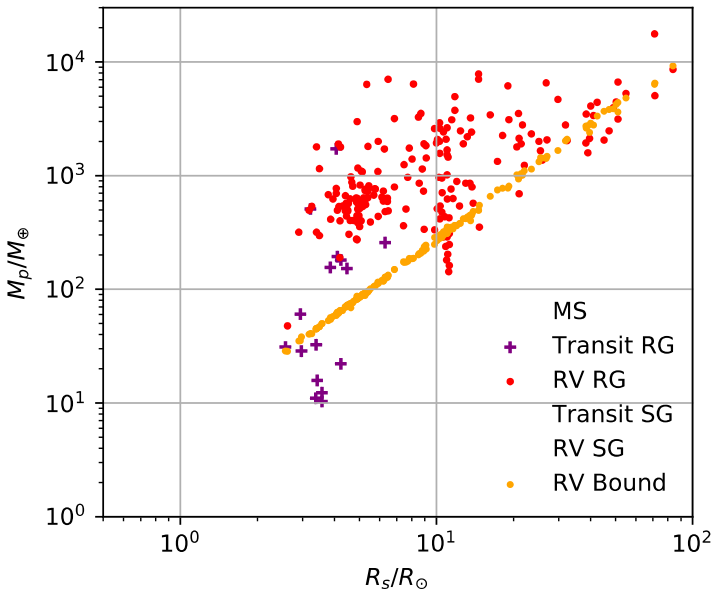

Figure 2. M_P vs. R_s plot for MS (blue dots), SG, and RG hosted planets discovered by RV (blue, red) and transit (brown +, purple +) methods. Orange dots represent minimum M_P for each red giant that can lead to RV amplitude greater than the stellar intrinsic level obtained by Hekker et al. 2008 [Cf. Eq. (3)].

Preprints (www.preprints.org) | NOT PEER-REVIEWED | Posted: 19 October 2023 doi:10.20944/preprints202310.1187.v1

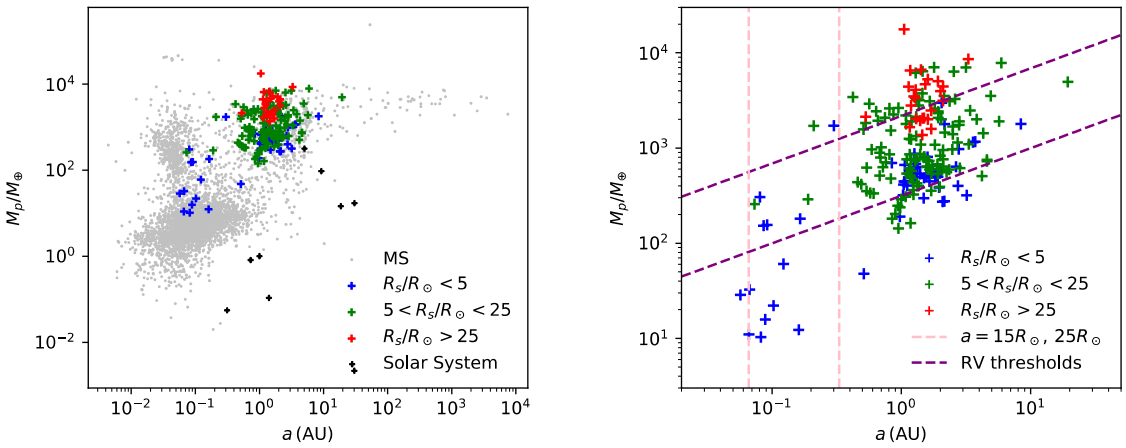

Figure 3. a, 3b. Left panel (a): M_P vs. a plot for main-sequence (silver), Red Giant planets (blue for $R_s/R_\odot < 5$, green for $5 < R_s/R_\odot < 25$, and red for $R_s/R_\odot > 25$), as well as Solar System planets (black). Right panel (b): zoomed-in version for Red Giant planets, with Kernel Density Estimate contours also shown. Pink dashed lines show $a = 15R_\odot$ and $a = 75R_\odot$, and purple lines are obtained from Equation (4), for $M_s = M_\odot$ and $R_s = 3R_\odot$ (lower line) and $R_s = 25R_\odot$ (upper line).

In Figure 3a and 3b, we split R_s into three different intervals and plot MS/SG (silver dots) and RG planets in each interval separately as planet mass M_P (in Earth masses) vs. orbital semi-major axis a (in astronomical units). In particular, we separate RG planets into three categories according to R_s: $R_s/R_\odot < 5$ (blue dots), $5 < R_s/R_\odot < 25$ (green dots), and $R_s/R_\odot > 25$ (red dots). The (a, M_P) region occupied by RG planets shrinks as R_s increases — from its left side, with small a, from the bottom side, with low M_P, and from the right side, with large a. This shrinkage is best viewed from the right (b) panel of Figure 3, which focuses on the specific region of RG planets and adds contours generated via Kernel Density Estimate (KDE) for clarity. In Figure 4, we plot the orbital semi-major axis vs. stellar radius ratioed to solar radii.

At this stage, it is useful to point out the relation between Figures 2, 3, and 4. In Figure 3b, we separate the evolution of R_s into three bins (stages) and illustrate the lumped joint (a, M_P) distribution in each bin (stage). Figure 2 and Figure 4 each separately illustrates the continuous evolutions of the marginal distributions of M_P and a, respectively, as R_s increases, The step-wise shrinkage of (a, M_P) distribution as we progress from blue to green and to red, are continuously represented in Figure 4 for a and in Figure 2 for M_P.

Preprints (www.preprints.org) | NOT PEER-REVIEWED | Posted: 19 October 2023 doi:10.20944/preprints202310.1187.v1

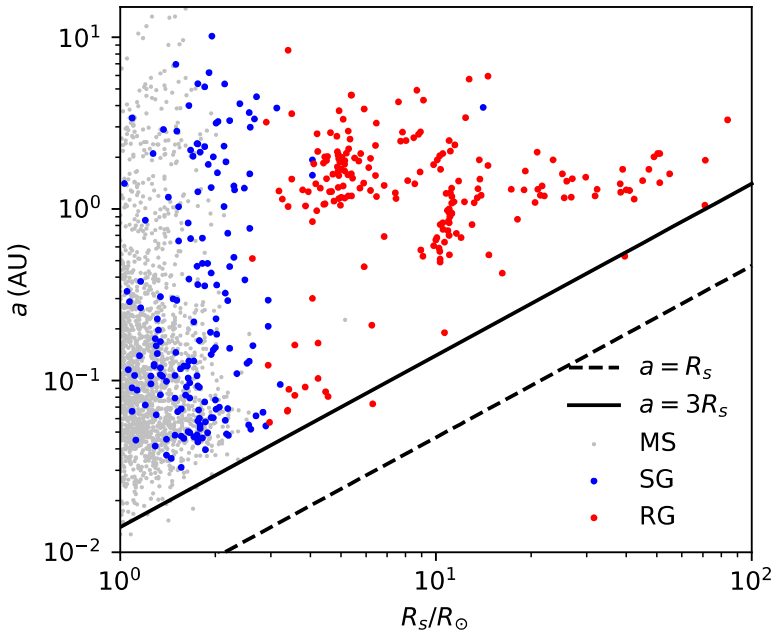

Figure 4. a vs. R_s plot for exoplanets around Red Giants (red dots), exoplanets around SG (blue dots, and exoplanets around MS Hosts (silver dots). Solid line indicates $a = 3R_s$, while dashed line indicates $a = R_s$.

2.2. Interpretations of the Evolutions in Population

In the following, we shall address the disappearance of planets with low semi-major axis (left side in Fig 3b), low mass (bottom side in Fig 3b), and high semi-major axis (right side in Fig 3b) separately.

For disappearance of planets with low semi-major axis, it is straightforward to anticipate planets with small orbital distance values to be engulfed and consumed as their host evolves and expands. According to Villaver et al. 2014, tidal interactions tend to speed up the engulfment of planets, and no planets should survive once $a/R_s < 3$. In Figure 4, we plot the orbital semi-major axis vs. stellar radius ratioed to solar radii, clearly illustrating that $a/R_s = 3$ is a cutoff and providing empirical evidence for tidally-accelerated engulfment. Correspondingly, in Figure 3b, we plot pink dashed lines to represent $a = 15R_\odot$ and $a = 75R_\odot$. These two lines indeed bound the green ($5R_\odot<R_s<25R_\odot$) and red ($R_s>25R_\odot$) populations from the left, respectively. As the stars evolve, this *engulfment cutoff* moves continuously along a.

Regarding the disappearance of low-mass planets with increasing R_s, we can see from Figure 3a that for stars with a radius less than $25R_\odot$ many planets with masses 200 to $1000M_\oplus$ exist at distances 2 to 3 AU. Yet, such planets are not seen orbiting stars with $R_s > 25R_\odot$ --- even though much more massive planets are seen at the same distance. This disappearance of low-mass planets with increasing R_s corresponds directly from the M_p vs. R_s power-law fit obtained by Jiang and Zhu 2018. Note that Solar System planets lie on the lower part of the plot; only Jupiter is near the reach of current detection methods. However, Jovian mass exoplanets and comparable orbital distance (~5 AU) are not seen around Red Giants with $R_s/R_\odot > 25$.

This disappearance can be explained using the limitations to the Radial Velocity (RV) method arising from the intrinsic oscillations of evolved stars (Hekker et al. 2008). Such oscillations have also been claimed to have led to false positives for exoplanets around RGs (Reichert et al. 2019). Hekker et al. 2008, who noticed that for stars with lower surface gravity g (i.e., larger radii), their measured minimum amplitudes of RV variations tend to increase, given approximately by

$$K_1^{\text{int}} = 2 \times 10^3 \, [g/(\text{cm/s}^2)]^{-0.6} \text{m/s}, \qquad (3)$$

Preprints (www.preprints.org) | NOT PEER-REVIEWED | Posted: 19 October 2023 doi:10.20944/preprints202310.1187.v1

which they interpret as arising from intrinsic fluctuations of the star. Here, g is the surface gravitational acceleration of the star. For each RG, assuming e = 0, we obtain the minimum planet mass $M_{\rm p}^{\rm min}$ the star can host, this in order for the K_1 due to the planet to be greater than the intrinsic $K_1^{\rm int}$:

$$M_{\rm p}^{\rm min} = \sqrt{\frac{aM_s}{G}} K_1^{\rm int}. \quad (4)$$

In Figure 3b, we plot this minimum planet mass as a function of a, assuming $M_s = 1M_\odot$ for $R = 5R_\odot$ and $R = 25_\odot$ in purple dashed lines. These RV cutoffs approximately indicate the trend in which planets are cut off from the bottom, and to a lesser extent, the right.

We may further replace a in Equation (4) by its minimum value of $3R_s$ before engulfment, obtaining $M_{\rm p}^{\rm min}$ for each R_s, which is plotted as orange dots in Figure 2. In this plot, the RV cutoff indeed provides an excellent lower bound for the masses of planets detected using the RV method (red and blue dots) around substantially evolved stars.

Although the two cutoffs arise from different physical mechanism, given a particular population of planets, they do not act independently from each other; they have different efficiencies in cutting off populations depending on the distribution of planets in the a, $M_{\rm P}$ space. For example, since planets with smaller a tend to be low in $M_{\rm P}$, they are less detectable by the RV method. Furthermore, for planets subject simultaneously to the engulfment and RV cutoffs, it is unclear whether they are actually engulfed or just unseen. Nevertheless, we would like to point out the region in Figure 3b bounded by the two pink lines and the upper purple line. The planets in this region represent a population that should be visible by the RV method, yet they are predicted to be engulfed by the $a = 3R_\odot$ criterion. More specifically, we do see two planets with $R_s < 25R_\odot$ host stars, yet the $R_s > 25R_\odot$ population does not extend here. This provides some evidence that engulfment can indeed be taking place, and does contribute *nontrivially* to the shrinkage of the (a, $M_{\rm P}$) distribution from the left. However, better detection methods not subject to the RV cutoff will be needed to more accurately study the engulfment phenomenon.

The disappearance of high semi-major axis planets as the star evolves cannot be fully explained with only the discussions above. As seen in Figure 3b, the red population has more concentrated values of a than simply applying the engulfment cutoff (the right pink line) and RV cutoff (the upper purple line) to the green and blue populations. Since orbital semi-major axis is highly correlated with orbital period due to the similarity in masses, our concentration in a is the same as the concentration of orbital periods (between 300 days and 800 days) for exoplanets around Red Giants with $R_s > 21R_\odot$, pointed out by D&H.

D&H argued that since the range of period falls within the period of intrinsic variations of stars (as modeled by Saio et al. 2015), and hence a fraction of these may not be actual planets. On the other hand, they provided plausible reasons for planets outside of this period range not to be discovered. For longer periods (corresponding to larger a), this could be due to the smaller RV variation being hidden under intrinsic fluctuations of the surface of the host star. For shorter periods (corresponding to smaller a), this could be due to the engulfment of planets by their host stars. Our discussions above quantitively explored these possibilities proposed by D&H. As we have seen, the engulfment and RV limitations do explain to some extent, but not completely, the concentration of periods described by D&H. In this way, our study lends support to D&H's suggestion that some of these planets can be false alarms.

Disappearance of large a planets can also be explained from the inward migration of hosted planets, especially because large R_s systems tend to be older, therefore the planets had more time to migrate. Finally, the fact that the more evolved host stars in our data tend to have lower metallicity and are older aged, and therefore were apt to have differently characterized populations of planets formed around them. However, such differences will likely have to be very substantial to be influential in this respect.

Preprints (www.preprints.org) | NOT PEER-REVIEWED | Posted: 19 October 2023 doi:10.20944/preprints202310.1187.v1

3. Habitable Planets Around Red Giants

In this section, we discuss the habitability of planets around RG and SG stars, briefly reviewing habitability criteria in 3.1, and presenting our findings in 3.2.

3.1. Criteria for Habitability

There exist multiple habitability conditions for a given exoplanet (or exomoon); most of which rely on the existence of water in liquid form to be present on at least a portion of that world's surface. The simplest criterion uses equilibrium temperature, namely, the black-body radiation from the planet has to balance the radiation it absorbs from the star. If we define S as the flux of radiation from the host, this given by

$$S = \frac{L_S}{4\pi a^2} \qquad (5)$$

where L_s is the star's luminosity and a is the orbital semi-major axis of the star's exoplanet, the equilibrium temperature of the exoplanet is then given by

$$T_{\text{eq}} = k\left[\frac{S(1-A)}{4\sigma}\right]^{1/4} \qquad (6)$$

where A is the planetary albedo and σ is the Stefan-Boltzmann constant. The simplest habitability condition is $273\,\text{K} < T_{\text{eq}} < 373\,\text{K}$, with the low T_{eq} defining the Outer boundary of the Habitable Zone (OHZ) and the high T_{eq} defining the Inner boundary of the Habitable Zone (IHZ). The scalar quantity k is a correction factor that can be used to approximately incorporate the greenhouse effect of an assumed planetary atmosphere, see Selsis et al. 2007. We adopt the Earth albedo of A=0.3 and use k=1.13, which reproduces the Earth surface temperature.

Table 1. Fitting parameters S_0, a, b, c and d adapted from previous study (Kopparapu et al. 2013).

	S_0	a	b	c	d
Recent Venus (optimistic inner boundary)	1.7753	1.4316×10^{-4}	2.9875×10^{-9}	-7.5702×10^{-12}	-1.1635×10^{-15}
Moist Green House (conservative inner boundary)	1.0140	8.1774×10^{-5}	1.7063×10^{-9}	-4.3241×10^{-12}	-6.6462×10^{-16}
Maximum Green House (conservative outer boundary)	0.3438	5.8942×10^{-5}	1.6558×10^{-9}	-3.0045×10^{-12}	-5.2983×10^{-16}
Early Mars (optimistic outer boundary)	0.3179	5.4513×10^{-5}	1.5313×10^{-9}	-2.7786×10^{-12}	-4.8997×10^{-16}

More realistic criteria exist in the literature. In this paper, we shall adopt two criteria obtained by previous study (Kopparapu et al. 2013) in which an *effective* solar flux is expressed in terms of

$$S_{\text{eff}} \equiv S/S_{\oplus} \qquad (7)$$

where $S_{\oplus}$ is the current solar energy flux at the location of the Earth, as well as the temperature T of the host star. Note that S_{eff} is dimensionless. In this paper, we shall adopt two different ways to define HZ boundaries, one conservative, the other optimistic. The conservative HZ accounts for greenhouse effects in the atmosphere of the planet, taking the inner boundary to be defined by the moist

Preprints (www.preprints.org) | NOT PEER-REVIEWED | Posted: 19 October 2023 doi:10.20944/preprints202310.1187.v1

greenhouse effect where S_{eff} allows sufficient water vapor to exist in the stratosphere. The outer boundary is defined by the maximum heat retained by the planet while still providing habitable conditions. This is also known as the maximum greenhouse effect.

We also summarized the boundaries using the following fitting formula (Kopparapu et al. 2013) for the host star temperature range of 2600 K < T < 7200 K:

$$S_{\text{limit}}(T) = S_0 + aT_* + bT_*^2 + cT_*^3 + dT_*^4,\ T_* = T/K - 5780\,, \qquad (8)$$

where values of a, b, c and d for conservative/optimistic, inner/outer boundaries are reproduced in Table 1. Parameters in equation (8) are all dimensionless. As noted in Table 1, a more optimistic approach uses the (theorized) history of Solar System planets Venus and Mars to determine the inner and outer bounds of the HZ. Here, the inner boundary of the HZ is based on the assertion that Venus has not had liquid water on its surface for only the past billion years – i.e., a billion years ago (recent) Venus might have had surface conditions suitable for water to exist. On the other hand, there is mounting evidence that (early) Mars had liquid water flowing on its surface 3.8 billion years ago. For these reasons, they define the inner boundary using the S_{eff} of recent Venus and the outer boundary using the S_{eff} of early Mars.

In Table 2, we list conservative and optimistic habitable zone RG-hosted planets. All planets are gas giants with masses ranging from 1 to 22 Jupiter masses (M_J). In the third and fourth columns, we list the spectral type and absolute V magnitude (obtained from apparent V-magnitude and distance data from NEA) of the host stars obtained from the NEA. Note that spectral type quoted here are not always consistent with other sources, and that classifications of stars using these values here may not be always consistent with our classification from the positions of the stars in the HR diagram (Fig 1). The hosts of planets in Table 2 are also shown as green dots in the H-R diagram of Figure 1. As can be readily perceived from Table 2 and Figure 1, these host stars are all in their early stages of evolution.

Table 2. a. Conservative (shaded, 4) and optimistically (unshaded, 5) habitable planets around Red Giants using the Kopparapu et al. 2013 criterion.

Planet Name	Discovery Paper	Spectral Type (NEA)	Abs Mag (V)	Host Mass ($M/M_\odot$)	Host Radius ($R/R_\odot$)	Orbital Period (days)	S_{eff}	Planet Mass (M_J)
HD 1605 c	Harakawa et al. 2015	K1 IV	2.78	1.33	3.49	2149	0.50	3.62
HD 219415 b	Gettel et al. 2012	K0 III	2.82	1	2.9	2093.3	0.41	1
HD 4732 c	Sato et al. 2013	K0 IV	2.21	1.74	5.4	2732	0.73	2.37
HIP 56640 b	Jones et al. 2021	K1 III	2.50	1.04	4.93	2574.9	0.81	3.67
HD 125390 b	Luhn et al. 2019	G7 V	2.28	1.36	6.47	1756.2	1.33	22.16
HD 145934 b	Feng et al. 2015	K0	1.71	1.75	5.38	2730	1.07	2.28
HD 94834 b	Luhn et al. 2019	K0	2.64	1.11	4.2	1576	1.31	1.26
HD 95089 c	Bryan et al. 2016	G8/K0 IV	2.24	1.54	5.08	1785	1.20	3.45
HIP 67851 c	Jones et al. 2015	K0 III	2.14	1.63	5.92	2131.8	1.20	6.3

Table 2. b. Conservative (shaded, 17) and optimistically (unshaded, 4) habitable planets around Subgiants using the Kopparapu et al. 2013 criterion.

Planet Name	Discovery Paper	Spectral Type (NEA)	Abs Mag (V)	Host Mass ($M/M_\odot$)	Host Radius ($R/R_\odot$)	Orbital Period (days)	S_{eff}	Planet Mass (M_J)
HD 103891 b	Sreenivas et al. 2022	F9	2.87	1.28	2.22	1,919	0.57	1.44
HD 10442 b	Giguere et al. 2015	K0 IV	2.17	1.01	1.97	1,032	0.51	1.487

Preprints (www.preprints.org) | NOT PEER-REVIEWED | Posted: 19 October 2023 doi:10.20944/preprints202310.1187.v1

HD 106270 b	Johnson et al. 2011	G5 IV	2.72	1.39	2.66	1,888	0.51	10.13
HD 10697 b	Vogt et al. 2000	G5 IV	3.68	1.13	1.79	1,076	0.65	6.383
HD 13167 b	Luhn et al. 2019	G3 V	2.48	1.35	2.39	2,613	0.54	3.31
HD 159868 b	O'Toole et al. 2007	G5 V	3.50	1.19	2.13	1,184	0.67	2.218
HD 163607 c	Giguere et al. 2012	G5	3.84	1.12	1.76	1,272	0.46	2.201
HD 175167 b	Arriagada et al. 2010	G5 IV/V	3.75	1.37	1.75	1,290	0.50	8.97
HD 18015 b	Luhn et al. 2019	G6 IV	2.43	1.49	3.13	2,278	0.63	3.18
HD 214823 b	Diaz et al. 2016	G0	3.03	1.31	2.04	1,854	0.45	20.3
HD 221585 b	Diaz et al. 2016	G8 IV	3.72	1.19	1.85	1,173	0.50	1.61
HD 38529 c	Fischer et al. 2001	G4 IV	2.79	1.41	2.56	2,136	0.51	12.99
HD 5319 b	Robinson et al. 2007	G5	2.63	1.27	4.06	637	0.57	1.556
HD 5319 c	Giguere et al. 2015	G5	2.63	1.27	4.06	872	0.38	1.053
HD 73534 b	Valenti et al. 2009	G5	3.63	1.16	2.58	1,750	0.37	1.112
HD 9174 b	Jenkins et al. 2017	G8 IV	3.84	1.03	1.67	1,179	0.50	1.11
Kepler-1704 b	Dalba et al. 2021		3.78	1.13	1.7	989	0.69	4.15
HAT-P-13 c	Bakos et al. 2009	G4	3.46	1.32	1.76	446	1.40	14.28
HD 156411 b	Naef et al. 2010	F8 IV/V	2.90	1.25	2.16	842	1.52	0.74
HD 4203 b	Vogt et al. 2002	G5	4.15	1.25	1.42	432	1.43	2.23
HD 48265 b	Minniti et al. 2009	G5 IV/V	3.27	1.31	1.9	779	1.17	1.525

3.2. Red Giant Planets in the Habitable Zones

From the NASA Exoplanet Archive, we collected values for stellar luminosity and orbital semi-major axis to calculate S_{eff}. In Figure 5, we show the Red Giant planets on the T_{eff} vs. S_{eff} plot with lines indicating HZ boundaries. From the plot, it can be seen that there is a substantial difference between boundaries for the T_{eq} HZ and Kopparapu HZ. We highlighted Kopparapu et al. 2013 optimistically habitable planets in green.

Figure 6 shows Red Giant and Main Sequence planets on a semi-major axis vs. stellar radius plot with habitable planets indicated (light green dots for habitable planets around MS stars, and cyan dots for those around SGs, and dark green those around RGs). We also indicate, with purple line segments, the optimistic HZ of the host stars of all planets around RGs. As illustrated, habitable planets --- and indeed habitable zones --- tend to have increasing a as R_s increases, this is attributable to stars with larger radii --- and thus greater luminosity --- having HZs farther out. For detected HZ planets, they have a maximum R_s of ~ $8R_\odot$, far below the maximum R_s of Red Giants, in this way, habitable planets so far discovered are either orbiting SG, or RG at their early stages of evolution.

As stars evolve beyond $8R_\odot$, the HZ extends to larger a, beyond the region in which planets have been detected orbiting RGs. Around MS stars, planets do exist in this region, as is the case for the outer planets of the solar system (see Figure 3). Therefore, such planets might exist around RGs, even though they are not yet detectable.

Preprints (www.preprints.org) | NOT PEER-REVIEWED | Posted: 19 October 2023 doi:10.20944/preprints202310.1187.v1

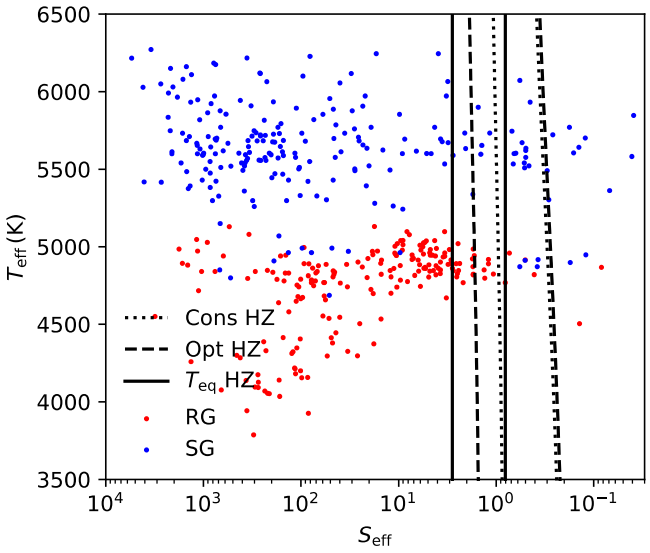

Figure 5. $T_{\rm eff}$ vs. $S_{\rm eff}$ plot for exoplanets around RG (red dots) and exoplanets around SG (blue dots). Boundaries for $T_{\rm eq}$, conservative and optimistic HZ are shown in solid, dotted and dashed lines, respectively.

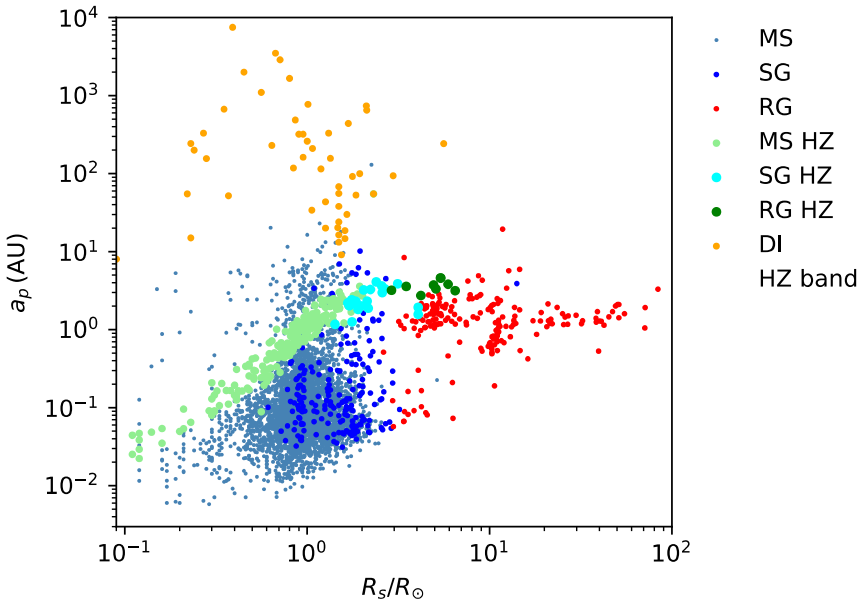

Figure 6. Semi-major axis a vs. stellar radius R_s plot of Red Giant (red) and Main Sequence planets (blue) with optimistically habitable planets in green (light green for Main Sequence and darker green for Red Giant planets.) Planets discovered by Direct Imaging (DI) are shown in orange. With purple vertical line segments, we indicate the optimistic HZ of each giant.

For Main Sequence hosts, planets with the longest semi-major axes were all discovered by direct imaging (yellow dots in Figure 6). However, using the same detection method to find similar planets around RGs may be difficult due to the direct imaging method disfavoring systems with large contrast. More specifically, the contrast between a one solar-mass giant star and a potential planet is about 5 magnitudes larger that between a one-solar-mass main sequence star and a potential planet. In this way, the direct imaging method is not (yet) sufficient to detect planets around giant stars.

Preprints (www.preprints.org) | NOT PEER-REVIEWED | Posted: 19 October 2023 doi:10.20944/preprints202310.1187.v1

4. Conclusions and Discussions

In this paper we take new data from NASA's Exoplanet Archive to update and further investigate trends regarding Red Giant systems. First, we revisit the Planet Mass-Stellar Radius relation previously found (Jiang and Zhu 2018). To further explore this trend, we separate Red Giant hosted exoplanets according to the radii of their hosts and plot planet mass against semi-major axis (Figure 3). As stellar radius increases, the region occupied by planets in the graph shrinks and for planets with smaller orbital semi-major axes, we found their disappearance to be consistent with tidal engulfment of planets where $a/R_s < 3$ (Figure 4).

For the disappearance of planets with lower masses and those with larger orbital semi-major axes, this disappearance could be due to observational selection effects of the radial velocity method used to discover the vast majority of planets in these regions. Since lower mass and larger orbital semi-major axis correspond to lower amplitudes of radial velocity, the disappearance can be attributed to a higher detection threshold for the amplitude of radial velocity oscillations among more evolved Red Giants. We showed that in order for this selection effect to be the origin of such disappearance, the level of intrinsic RV fluctuation of Red Giants should depend on surface gravity following equation (3), which was proposed by Hekker et al. 2018. However, selection effects may also arise due to eccentricity and stellar mass. As this possibility is beyond the scope of this paper, further investigations of the origin of such selection effects are left to future studies.

Next, we examine the habitability of Red Giant exoplanets. To determine the habitable zone, we adopt criteria proposed by Kopparapu et al. 2013 and with this method found ten planets in the optimistic HZ, five of which are in the conservatively calculated HZ. However, all of these planets are gas giants and, therefore, very likely uninhabitable by life as we presently know it. Nevertheless, these planets may themselves host habitable exomoons. Even though a planet might be within the HZ at the moment, its total lifetime within the HZ may or may not be long enough for life to develop. As Ramirez and Kaltenegger 2016 have shown, depending on the planet-star configuration, a planet can stay for 0.2 – 9 Gyr in the post-MS HZ of a star, which does provide hope for life to develop on its moon. An obvious next step of research is to find out how long each of the planets in Table 2a and 2b had been in the HZ. For the solar system, on the other hand, Sparrman had shown that none of the outer planets will stay long enough in in the post-MS HZ of the sun for life to independently develop. Regardless of the time scale here, one can also speculate on the more exotic scenarios where life could have been hidden under the surface of the moons, or could move from nearby habitable planets to the outer planets as the host star evolves.

Finally, with habitable zone exoplanets identified, we revisited the issue of detection bias. We see that their orbital semi-major axis increases with stellar radii until $R_s/R_\odot \sim 8$. However, this does not necessarily rule out further habitable zone exoplanets and it is very likely there are more HZ Red Giant exoplanets with a semi-major axis greater than ~ 4 AU. Even though some such planets can be seen around Main Sequence stars via direct imaging, similar planets around Red Giant stars have not yet been found. While the limitations of current imaging methods may preclude detecting planets around Red Giant stars, more advanced instrumentation coming online in the near term may enable this technique to be used for at least some Red Giant hosted exoplanetary systems. The next generation of space telescopes, such as the Habitable World Observatory (Gaudi et al. 2018), will have enhanced capabilities and will be able to observe smaller planets including those planets around Red Giant stars. In addition to static spectroscopy, it will be possible to observe variation in the reflected starlight spectra while the planet rotates around its axis. As in the case of the Earth, the surface of a rocky exoplanet is not expected to be homogeneous (if it has oceans, lands, forests, and deserts), nor is the cloud distribution (Li et al. 2022 and Jiang et al. 2018). These factors will have an impact on the time series of the exoplanetary spectrum.

Acknowledgements: This research was conducted at the NASA sponsored Jet Propulsion Laboratory, California Institute of Technology (Caltech) and has made use of the NASA Exoplanet Archive, which is operated by the Caltech, under contract with the NASA under the Exoplanet Exploration Program.

Preprints (www.preprints.org) | NOT PEER-REVIEWED | Posted: 19 October 2023 doi:10.20944/preprints202310.1187.v1

Data Statement: The data underlying this article can be downloaded from the NASA exoplanet archive at https://exoplanetarchive.ipac.caltech.edu. The method of data calculation and analysis are fully described in the article.

Author Contributions: Conceptualization, J.H.J.; methodology, J.H.J., R.E.C; software, R.E.C and J.H.J; validation, J.H.J. and Y.C.; formal analysis, R.E.C and J.H.J.; investigation, R.E.C., J.H.J. and P.E.R.; resources, J.H.J.; data curation, R.E.C and J.H.J.; writing—original draft preparation, R.E.C.; writing—review and editing, J.H.J., P.E.R., and K.A.F; visualization, R.E.C and J.H.J; supervision, J.H.J. and Y.C.; project administration, J.H.J.; funding acquisition, J.H.J. All authors have read and agreed to the published version of the manuscript.

Competing Interest: Authors declare no competing interest.

Appendix. Exoplanets around Red Giants and Sub Giants from the NASA Exoplanet Archive

Table A1. Exoplanets hosted by Red Giants from the NASA Exoplanet Archive (a total of 210 planets).

Planet Name	M_s ($M_\odot$)	R_s ($R_\odot$)	a (AU)	M_p (M_J)	Planet Name	M_s ($M_\odot$)	R_s ($R_\odot$)	a (AU)	M_p (M_J)	Planet Name	M_s ($M_\odot$)	R_s ($R_\odot$)	a (AU)	M_p (M_J)
11 Com b	2.7	19	1.29	19.4	HD 177830 c	1.47	2.62	0.5137	0.15	HD 95127 b	3.7	41.01	1.28	10.63
11 UMi b	2.78	29.79	1.53	14.74	HD 180053 b	1.75	4.06	0.843	2.194	HD 96063 b	1.37	4.75	1.11	1.27
14 And b	2.2	11	0.83	4.8	HD 180314 b	2.2	8.13	1.46	20.13	HD 96127 b	10.94	51.1	1.42	20.96
17 Sco b	1.22	25.92	1.45	4.32	HD 180902 b	1.41	4.16	1.4	1.685	HD 96992 b	0.96	7.43	1.24	1.14
18 Del b	2.3	8.5	2.6	10.3	HD 181342 b	1.69	4.71	1.592	2.54	HD 98219 b	1.41	4.6	1.26	1.964
24 Boo b	0.99	10.64	0.19	0.91	HD 18742 b	1.36	5.13	1.82	3.4	HD 99283 b	1.76	11.21	1.08	0.97
24 Sex b	1.54	4.9	1.333	1.99	HD 192699 b	1.38	4.41	1.063	2.096	HD 99706 b	1.46	5.52	1.98	1.23
24 Sex c	1.54	4.9	2.08	0.86	HD 200964 b	1.39	4.92	1.565	1.599	HD 99706 c	1.72	5.4		5.69
4 UMa b	1.23	18.11	0.87	7.1	HD 200964 c	1.39	4.92	1.96	1.214	HIP 105854 b	2.1	10.31	0.81	8.2
42 Dra b	0.98	22.03	1.19	3.88	HD 202696 b	1.91	6.43	1.566	1.996	HIP 107773 b	2.42	11.6	0.72	1.98
6 Lyn b	1.44	5.2	2.11	2.01	HD 202696 c	1.91	6.43	2.342	1.864	HIP 114933 b	1.39	5.27	2.84	1.94
7 CMa b	1.34	4.87	1.758	1.85	HD 206610 b	1.55	6.12	1.74	2.036	HIP 56640 b	1.04	4.93	3.73	3.67
7 CMa c	1.34	4.87	2.153	0.87	HD 208527 b	1.6	51.1	2.1	9.9	HIP 63242 b	1.54	10.28	0.565	9.18
75 Cet b	2.49	10.5	2.1	3	HD 208897 b	1.25	4.98	1.05	1.4	HIP 65891 b	2.5	8.93	2.81	6
8 UMi b	1.44	10.3	0.49	1.31	HD 210702 b	1.61	4.92	1.148	1.808	HIP 67537 b	2.41	8.69	4.91	11.1
81 Cet b	2.4	11	2.5	5.3	HD 212771 b	1.56	5.27	1.19	2.39	HIP 67851 b	1.63	5.92	0.46	1.38
91 Aqr b	1.4	11	0.7	3.2	HD 216536 b	0.81	9.83	0.61	1.05	HIP 67851 c	1.63	5.92	3.82	6.3

Preprints (www.preprints.org) | NOT PEER-REVIEWED | Posted: 19 October 2023 doi:10.20944/preprints202310.1187.v1

BD+03 2562 b	1.14	32.35	1.3	6.4	HD 219139 b	1.46	11.22	0.94	0.78	HIP 74890 b	1.74	5.77	2.1	2.4
BD+15 2375 b	1.08	8.95	0.576	1.061	HD 219415 b	1	2.9	3.2	1	HIP 75092 b	1.28	4.53	2.02	1.79
BD+15 2940 b	1.1	14.7	0.539	1.11	HD 220074 b	2.2	54.92	1.6	16.64	HIP 8541 b	1.17	7.83	2.8	5.5
BD+20 2457 b	10.83	71.02	1.05	55.59	HD 221416 b	1.21	2.94	0.1228	0.19	HIP 90988 b	1.3	3.94	1.26	1.96
BD+20 2457 c	2.8	49	2.01	12.47	HD 222076 b	1.07	4.1	1.83	1.56	HIP 97233 b	1.93	5.34	2.55	20
BD+20 274 b	0.8	17.3	1.3	4.2	HD 22532 b	1.57	5.69	1.9	2.12	IC 4651 9122 b	2.1	10.27	2.038	6.3
BD+48 738 b	0.74	11	1	0.91	HD 233604 b	1.5	10.9	0.747	6.575	K2-132 b	1.08	3.85	0.0916	0.49
BD+48 740 b	1.09	10.33	1.7	1.7	HD 238914 b	1.47	12.73	5.7	6	K2-161 b	0.99	2.57		0.0978
BD+49 828 b	1.52	7.6	4.2	1.6	HD 240210 b	0.82	25.46	1.16	5.21	K2-39 b	0.66	2.97	0.05708	0.09
BD-13 2130 b	2.12	19.17	1.66	9.78	HD 240237 b	8.76	71.23	1.92	15.89	K2-97 b	1.2	4.47	0.086	0.48
HD 100655 b	2.28	10.06	0.68	1.61	HD 24064 b	1.61	40	1.29	12.89	Kepler-1004 b	1.11	3.39	0.0671	0.102
HD 102272 b	1.45	10.3	0.51	4.94	HD 25723 b	2.12	13.76	1.49	2.5	Kepler-1270 b	1.28	3.38	0.0663	0.0346
HD 102329 b	3.21	9.82	1.81	8.16	HD 27442 b	1.23	3.18	1.271	1.56	Kepler-391 b	1.03	3.57	0.082	0.0325
HD 102329 c	1.3	6.3		1.52	HD 28678 b	1.53	6.48	1.18	1.542	Kepler-391 c	1.03	3.57	0.161	0.0386
HD 102956 b	1.66	4.55	0.0807	0.96	HD 29399 b	1.17	4.5	1.913	1.57	Kepler-432 b	1.32	4.06	0.301	5.41
HD 104985 b	2.3	11	0.95	8.3	HD 2952 b	1.97	10.76	1.23	1.37	Kepler-432 c	1.32	4.06		2.43
HD 108863 b	1.59	5.74	1.32	2.414	HD 30856 b	1.17	4.4	1.85	1.547	Kepler-56 b	1.32	4.23	0.1028	0.07
HD 10975 b	1.41	11.16	0.95	0.45	HD 32518 b	1.13	10.22	0.59	3.04	Kepler-56 c	1.32	4.23	0.1652	0.57
HD 110014 b	2.17	20.9	2.14	11.09	HD 33142 b	1.41	4.45	1.07	1.385	Kepler-56 d	1.29	4.22	2.16	5.61
HD 111591 b	1.94	8.03	2.5	4.4	HD 33142 c	1.62	4.14		5.97	Kepler-815 b	1.25	3.42	0.0888	0.0498
HD 112640 b	1.8	39	1.7	5	HD 33844 b	1.84	5.39	1.6	2.01	Kepler-91 b	1.31	6.3	0.0731	0.81
HD 113996 b	1.49	25.11	1.6	6.3	HD 33844 c	1.78	5.29	2.24	1.75	NGC 2682 Sand 364 b	9.06	39.59	0.53	6.69
HD 116029 b	0.83	4.89	1.65	1.4	HD 360 b	1.69	10.86	0.98	0.75	NGC 2682 Sand 978 b	1.37	21.02		2.18

Preprints (www.preprints.org) | NOT PEER-REVIEWED | Posted: 19 October 2023 doi:10.20944/preprints202310.1187.v1

HD 116029 c	1.33	4.6		1.27	HD 40956 b	2	8.56	1.4	2.7	TOI-2337 b	1.32	3.22		1.6
HD 11755 b	0.72	20.58	1.09	5.63	HD 4313 b	1.63	5.14	1.157	1.927	TOI-2669 b	1.19	4.1		0.61
HD 11977 b	1.91	10.09	1.93	6.54	HD 4732 b	1.74	5.4	1.19	2.37	TYC 0434-04538-1 b	1.04	9.99	0.66	6.1
HD 120084 b	2.39	9.12	4.3	4.5	HD 4732 c	1.74	5.4	4.6	2.37	TYC 1422-614-1 b	1.15	6.85	0.69	2.5
HD 125390 b	1.36	6.47	3.16	22.16	HD 47366 b	2.19	6.2	1.28	2.3	TYC 1422-614-1 c	1.15	6.85	1.37	10
HD 12648 b	0.67	11.02	0.54	1.96	HD 47366 c	2.19	6.2	1.97	1.88	TYC 3318-01333-1 b	1.19	5.9	1.414	3.42
HD 131496 b	1.34	4.44	2.01	1.8	HD 47536 b	2.1	23.47	1.93	7.32	TYC 3667-1280-1 b	1.87	6.26	0.21	5.4
HD 13189 b	2.24	38.41	1.25	10.95	HD 4760 b	1.05	42.4	1.14	13.9	TYC 4282-00605-1 b	0.97	16.21	0.422	10.78
HD 136418 b	1.48	3.78	1.29	2.14	HD 4917 b	1.32	5.01	1.167	1.615	alf Ari b	1.5	13.9	1.2	1.8
HD 139357 b	1.35	11.47	2.36	9.76	HD 5583 b	1.01	9.09	0.53	5.78	alf Tau b	1.13	45.1	1.46	6.47
HD 14067 b	2.4	12.4	3.4	7.8	HD 5608 b	1.53	5.14	1.911	1.681	bet Cnc b	1.7	47.2	1.7	7.8
HD 142245 b	3.5	4.63	2.78	3.07	HD 5891 b	1.93	10.64	0.64	7.63	bet UMi b	1.4	38.3	1.4	6.1
HD 145457 b	1.23	10.52	0.76	2.23	HD 59686 A b	1.9	13.2	1.086	6.92	eps CrB b	1.7	21	1.3	6.7
HD 145934 b	1.75	5.38	4.6	2.28	HD 60292 b	1.7	27	1.5	6.5	eps Tau b	2.7	13.7	1.93	7.6
HD 14787 b	1.43	5.01	1.7	1.121	HD 62509 b	2	8.9	1.64	2.3	gam 1 Leo b	1.23	31.88	1.19	8.78
HD 148427 b	1.64	3.86	1.04	1.3	HD 64121 b	1.64	5.44	1.51	2.56	gam Cep b	1.4	4.9	2.05	9.4
HD 1502 b	1.46	4.67	1.262	2.75	HD 66141 b	1.1	21.4	1.2	6	gam Lib b	1.47	11.1	1.24	1.02
HD 152581 b	1.3	5.14	1.66	1.869	HD 69123 b	1.68	7.72	2.482	3.04	gam Lib c	1.47	11.1	2.17	4.58
HD 155233 b	1.69	5.03	2	2.6	HD 72490 b	1.21	4.96	1.88	1.768	gam Psc b	0.99	11.2	1.32	1.34
HD 158038 b	1.3	4.5	1.5	1.53	HD 75784 b	1.26	3.4	1.032	1	iot Dra b	1.54	11.79	1.453	11.82
HD 158996 b	1.8	50.3	2.1	14	HD 75784 c	1.26	3.4	8.4	5.64	iot Dra c	1.54	11.79	19.4	15.6

Preprints (www.preprints.org) | NOT PEER-REVIEWED | Posted: 19 October 2023 doi:10.20944/preprints202310.1187.v1

HD 1605 b	1.33	3.49	1.492	0.934	HD 76920 b	1.17	7.47	1.149	3.93	kap CrB b	1.5	4.85	2.65	2
HD 1605 c	1.33	3.49	3.584	3.62	HD 79181 b	1.28	11.06	0.9	0.64	mu Leo b	1.5	11.4	1.1	2.4
HD 161178 b	1.06	10.95	0.85	0.57	HD 81688 b	2.1	13	0.81	2.7	nu Oph b	2.7	14.6	1.79	22.206
HD 167042 b	1.72	4.3	1.32	1.7	HD 81817 b	4.3	83.8	3.3	27.1	nu Oph c	2.7	14.6	5.931	24.662
HD 1690 b	1.86	21.66	1.36	8.79	HD 82886 b	2.53	5.26	1.58	2.33	ome Ser b	2.17	12.3	1.1	1.7
HD 17092 b	6.73	13.58	1.31	10.13	HD 86950 b	1.66	8.8	2.72	3.6	omi CrB b	2.13	10.5	0.83	1.5
HD 173416 b	2	13.5	1.16	2.7	HD 94834 b	1.11	4.2	2.74	1.26	tau Gem b	2.3	26.8	1.17	20.6
HD 175541 b	1.39	4.19	0.975	0.598	HD 95089 b	1.54	5.08	1.36	1.26	ups Leo b	1.48	11.22	1.18	0.51

Table A2. Exoplanets hosted by Red Giants from the NASA Exoplanet Archive (a total of 229 planets).

Planet Name	M_s ($M_\odot$)	R_s ($R_\odot$)	a (AU)	M_p (M_J)	**Planet Name**	M_s ($M_\odot$)	R_s ($R_\odot$)	a (AU)	M_p (M_J)	**Planet Name**	M_s ($M_\odot$)	R_s ($R_\odot$)	a (AU)	M_p (M_J)
70 Vir b	1.09	1.89	0.481	7.49	K2-391 b	0.76	0.57		0.00772	Kepler-335 b	1.03	1.85	0.075	0.0359
BD+60 1417 b	1	0.8	1662	15	K2-399 b	0.78	1.54		0.0959	Kepler-335 c	1.02	1.85	0.356	0.0303
CoRoT-20 c	1.14	1.37	2.9	17	K2-60 b	0.97	1.12	0.045	0.426	Kepler-337 b	1.05	1.76	0.045	0.0094
CoRoT-26 b	1.09	1.79	0.0526	0.52	K2-99 b	1.63	2.63	0.1597	0.97	Kepler-337 c	1.05	1.76	0.093	0.0153
CoRoT-28 b	1.01	1.78	0.0603	0.484	KELT-11 b	1.44	2.69	0.06229	0.171	Kepler-363 b	1.1	1.49	0.048	0.00521
CoRoT-31 b	1.25	2.15	0.0586	0.84	KIC 8121913 b	1.46	2.23		2.1	Kepler-363 c	1.1	1.49	0.079	0.209
EPIC 248847494 b	0.9	2.7	4.5	13	KIC 9663113 b	0.98	1.03	1.4062	0.0603	Kepler-363 d	1.1	1.49	0.107	0.0153
EPIC 249893012 b	1.05	1.71	0.047	0.02753	Kepler-101 b	1.17	1.56	0.0474	0.16	Kepler-368 b	0.97	2.02	0.186	0.0336

Preprints (www.preprints.org) | NOT PEER-REVIEWED | Posted: 19 October 2023 doi:10.20944/preprints202310.1187.v1

EPIC 249893012 c	1.05	1.71	0.13	0.04616	Kepler-101 c	1.17	1.56	0.0684	0.01	Kepler-368 c	0.97	2.02	0.36	0.0451
EPIC 249893012 d	1.05	1.71	0.22	0.03203	Kepler-1078 b	0.94	0.92	0.0388	0.0134	Kepler-38 b	0.94	1.75	0.4632	0.384
HAT-P-13 b	1.32	1.76	0.04383	0.851	Kepler-108 b	1.25	2.19	0.292	0.176	Kepler-384 b	0.97	0.88	0.148	0.00459
HAT-P-13 c	1.32	1.76	1.258	14.28	Kepler-108 c	1.25	2.19	0.721	0.16	Kepler-384 c	0.97	0.88	0.236	0.00474
HAT-P-40 b	1.03	1.94	0.0608	0.48	Kepler-1080 b	1.1	1.16	0.3781	0.0339	Kepler-435 b	1.54	3.21	0.0948	0.84
HAT-P-65 b	1.21	1.86	0.03951	0.527	Kepler-1125 b	0.95	0.94	0.1348	0.0127	Kepler-458 c	1.15	2.22	0.154	0.0516
HATS-61 b	1.08	1.66	0.07908	3.4	Kepler-1135 b	0.96	0.94	0.3436	0.0128	Kepler-473 b	1.06	1.34	0.1186	0.0492
HATS-9 b	1.1	1.56	0.0312	0.837	Kepler-1142 b	0.97	0.96	0.1343	0.00869	Kepler-511 b	1	1.2	0.8589	0.104
HD 103891 b	1.28	2.22	3.27	1.44	Kepler-1207 b	1.06	1.06	0.1156	0.0102	Kepler-525 b	0.95	1.15	0.1396	0.0233
HD 10442 b	1.01	1.97	2.01	1.487	Kepler-1219 b	1.25	1.94	0.1418	0.0162	Kepler-628 b	1	1.28	0.1241	0.168
HD 106270 b	1.39	2.66	3.34	10.13	Kepler-1283 b	1.16	1.25	0.1062	0.0136	Kepler-638 b	0.88	0.93	0.0632	0.0126
HD 10697 b	1.13	1.79	2.14	6.383	Kepler-129 b	1.18	1.65	0.13	0.06293	Kepler-641 b	1.02	1.13	0.0879	0.0128
HD 114613 b	1.27	2.14	5.34	0.357	Kepler-129 c	1.18	1.65	0.39	0.13529	Kepler-643 b	1	2.52	0.126	1.01
HD 118203 b	1.84	2.06	0.07	2.79	Kepler-129 d	1.18	1.65	4	8.3	Kepler-667 b	0.91	0.87	0.2288	0.0632
HD 11964 b	0.91	2.01	3.16	0.622	Kepler-1296 b	0.87	0.83	0.0896	0.00218	Kepler-678 b	0.94	0.91	0.0732	0.0728
HD 11964 c	0.91	2.01	0.229	0.0788	Kepler-1304 b	0.85	0.81	0.1202	0.0184	Kepler-682 b	0.92	0.89	0.1058	0.134
HD 13167 b	1.35	2.39	4.1	3.31	Kepler-1311 b	1.05	1.4	0.0989	0.00651	Kepler-684 b	0.89	0.86	0.064	0.0354
HD 1397 b	1.32	2.34	0.1097	0.415	Kepler-1311 c	1.05	1.4	0.0368	0.00624	Kepler-698 b	0.94	0.91	0.1255	0.0413

Preprints (www.preprints.org) | NOT PEER-REVIEWED | Posted: 19 October 2023 doi:10.20944/preprints202310.1187.v1

HD 147873 b	1.38	2.29	0.522	5.14	Kepler-1311 d	1.03	1.67	0.6711	0.212	Kepler-699 b	0.81	0.78	0.1711	
HD 147873 c	1.38	2.29	1.36	2.3	Kepler-1330 b	0.97	0.94	0.0889	0.0106	Kepler-7 b	1.36	1.97	0.06067	0.441
HD 154857 b	1.96	2.3	1.29	2.45	Kepler-1336 b	0.94	1.3	0.1595	0.0144	Kepler-717 b	0.88	0.85	0.052	0.0203
HD 154857 c	1.72	1.76	5.36	2.58	Kepler-1336 c	0.94	1.3	0.0631	0.0112	Kepler-734 b	0.85	0.78	0.0583	0.039
HD 156411 b	1.25	2.16	1.88	0.74	Kepler-1380 b	0.96	0.94	0.0917	0.00829	Kepler-767 b	0.96	0.94	0.5874	0.112
HD 156668 b	0.77	0.72	0.05	0.013	Kepler-1385 b	1.15	1.29	0.0415	0.00171	Kepler-772 b	0.98	1.11	0.1071	0.0125
HD 159868 b	1.19	2.13	2.32	2.218	Kepler-1402 b	0.9	0.87	0.0322	0.00114	Kepler-784 b	1	1.32	0.1967	0.00982
HD 159868 c	1.19	2.13	1.032	0.768	Kepler-1425 b	0.97	0.95	0.1038	0.00245	Kepler-796 b	0.93	1.09	0.0662	0.00705
HD 163607 b	1.12	1.76	0.362	0.7836	Kepler-1428 b	1.28	1.36	0.1059	0.0105	Kepler-797 b	0.96	0.95	0.181	0.0168
HD 163607 c	1.12	1.76	2.39	2.201	Kepler-1436 b	1.06	1.09	0.0907	0.00714	Kepler-799 c	1.03	1.59	0.1214	0.0256
HD 168443 b	0.99	1.51	0.2931	7.659	Kepler-1437 b	0.93	0.9	0.0951	0.00771	Kepler-823 b	0.98	0.96	0.0507	0.00972
HD 168443 c	0.99	1.51	2.8373	17.193	Kepler-1440 b	0.98	0.96	0.2274	0.00669	Kepler-848 b	1.01	1.2	0.072	0.0111
HD 171028 b	1.53	2.47	1.32	2.62	Kepler-1468 d	1.07	1.5	0.1456	0.0349	Kepler-852 b	1.19	1.16	0.2654	0.022
HD 175167 b	1.37	1.75	2.4	8.97	Kepler-1484 b	0.94	0.92	0.1939	0.016	Kepler-87 b	1.1	1.82	0.481	1.02
HD 179079 b	1.14	1.63	0.1214	0.081	Kepler-1488 b	1.05	1.31	0.2285	0.013	Kepler-87 c	1.1	1.82	0.676	0.02
HD 18015 b	1.49	3.13	3.87	3.18	Kepler-1488 c	1	1.52	0.0658	0.0106	Kepler-891 b	1.06	1.07	0.2881	0.106
HD 185269 b	1.3	2	0.077	1.01	Kepler-1504 b	0.85	0.81	0.3704	0.0163	Kepler-896 b	0.84	0.81	0.5164	0.0218
HD 187085 b	1.19	1.27	2.1	0.836	Kepler-1506 b	0.95	0.93	0.1168	0.00724	Kepler-903 b	0.98	0.97	0.0907	0.0148

Preprints (www.preprints.org) | NOT PEER-REVIEWED | Posted: 19 October 2023 doi:10.20944/preprints202310.1187.v1

HD 202772 A b	1.72	2.59	0.05208	1.017	Kepler-1511 b	1.17	1.29	0.1753	0.0109	Kepler-903 c	0.98	0.97	0.302	0.0218
HD 206255 b	1.42	2.22	0.461	0.1076	Kepler-1562 b	1.02	1.05	0.3308	0.0388	Kepler-913 b	0.63	0.61	0.1009	0.0154
HD 214823 b	1.31	2.04	3.23	20.3	Kepler-1570 b	0.92	0.89	0.1784	0.0039	Kepler-917 b	0.8	0.76	0.0378	0.0136
HD 219077 b	1.05	1.91	6.22	10.39	Kepler-1572 b	0.97	0.95	0.0614	0.00245	Kepler-939 b	0.88	0.85	0.1153	0.0117
HD 221420 b	1.35	1.95	10.15	22.9	Kepler-1580 b	1.47	2.15	0.323	0.016	Kepler-943 b	0.93	0.91	0.2559	0.0928
HD 221585 b	1.19	1.85	2.306	1.61	Kepler-1596 b	0.95	0.92	0.3237	0.0134	NGTS-13 b	1.3	1.79	0.0549	4.84
HD 222155 b	1.21	1.85	5.14	2.12	Kepler-1605 b	0.86	0.82	0.3912	0.00403	TOI-1296 b	1.17	1.66	0.0497	0.298
HD 224693 b	1.31	1.93	0.191	0.7	Kepler-1625 b	0.96	0.94	0.8748	0.0962	TOI-1601 b	1.52	2.19	0.06864	0.99
HD 33283 b	1.38	1.97	0.1508	0.329	Kepler-1658 b	1.45	2.89	0.0544	5.88	TOI-172 b	1.13	1.78	0.0914	5.42
HD 38529 b	1.41	2.56	0.1294	0.797	Kepler-1704 b	1.13	1.7	2.026	4.15	TOI-1789 b	1.51	2.17	0.04882	0.7
HD 38529 c	1.41	2.56	3.64	12.99	Kepler-1719 b	1.08	1.77	0.0674	0.0465	TOI-2180 b	1.11	1.64	0.828	2.755
HD 38801 b	1.21	2.03	1.623	9.698	Kepler-1743 b	1.27	1.61	0.0822	0.01	TOI-2184 b	1.53	2.9		0.65
HD 4203 b	1.25	1.42	1.17	2.23	Kepler-1758 b	1.03	1.62	0.0919	0.0224	TOI-4329 b	1.54	2.31		0.45
HD 4203 c	0.99	1.5	6.95	2.17	Kepler-1772 b	0.94	0.93	0.0418	0.0242	TOI-481 b	1.14	1.66	0.097	1.53
HD 48265 b	1.31	1.9	1.814	1.525	Kepler-1827 b	0.92	1.4	0.0455	0.0129	TOI-813 b	1.32	1.94	0.423	0.114
HD 5319 b	1.27	4.06	1.57	1.556	Kepler-1843 b	1.02	1.78	0.171	0.0245	TOI-954 b	1.2	1.89	0.04963	0.174
HD 5319 c	1.27	4.06	1.93	1.053	Kepler-1888 b	0.9	1.25	0.0956	0.00729	V1298 Tau b	1.1	1.34	0.1688	0.236
HD 60532 b	1.5	2.57	0.77	1.06	Kepler-1921 b	1.25	2	0.1557	0.0274	V1298 Tau c	1.1	1.34	0.0825	0.0839

Preprints (www.preprints.org) | NOT PEER-REVIEWED | Posted: 19 October 2023 doi:10.20944/preprints202310.1187.v1

HD 60532 c	1.5	2.57	1.6	2.51	Kepler-1924 b	1.02	1.28	0.1216	0.0237	V1298 Tau d	1.1	1.34	0.1083	0.106
HD 73526 b	1.14	1.53	0.65	3.08	Kepler-1927 b	1.41	2.48	0.3859	0.0362	V1298 Tau e	1.1	1.34	0.308	0.179
HD 73526 c	1.01	1.53	1.03	2.25	Kepler-1929 b	1.01	1.47	0.2987	0.0304	WASP-105 b	0.89	0.9	0.075	1.8
HD 73534 b	1.16	2.58	2.99	1.112	Kepler-1949 b	1.19	1.45	0.0352	0.0175	WASP-11 b	1.42	0.89	0.0435	0.79
HD 87646 b	1.12	1.55	0.117	12.4	Kepler-1951 b	0.92	1.31	0.1435	0.0189	WASP-165 b	1.25	1.75	0.04823	0.658
HD 88133 b	1.26	2.2	0.0479	1.02	Kepler-238 e	1.06	0.96	0.1658	0.534	WASP-169 b	1.34	2.01	0.0681	0.561
HD 89345 b	1.16	1.75	0.1066	0.11	Kepler-238 f	1.06	0.96	0.2747	0.042	WASP-171 b	1.17	1.64	0.0504	1.084
HD 9174 b	1.03	1.67	2.2	1.11	Kepler-272 b	0.86	0.93	0.038	0.245	WASP-187 b	1.54	2.83	0.0653	0.8
HD 95544 b	1.09	1.09	3.386	6.84	Kepler-272 c	0.86	0.93	0.061	0.308	WASP-63 b	1.28	1.86	0.0574	0.37
HD 96167 b	1.27	1.94	1.332	0.717	Kepler-272 d	0.86	0.93	0.091	0.0179	WASP-71 b	0.76	1.82	0.04622	1.39
K2-108 b	1.17	1.76	0.0581	0.18689	Kepler-278 b	1.08	2.94	0.207	0.049	WASP-73 b	2.52	2.55	0.05512	2.86
K2-164 b	1.18	2.2		0.0334	Kepler-278 c	1.08	2.94	0.294	0.0396	YSES 2 b	1.1	1.19	115	6.3
K2-171 b	0.89	1.72		0.0242	Kepler-295 b	0.89	0.9	0.099	0.00624					
K2-238 b	1.19	1.59	0.046	0.86	Kepler-295 c	0.89	0.9	0.142	0.00537					

References

Arriagada, P, Butler, R.P, Minniti, D., et al. 2010, ApJ 711, 1229
Bakos G.A., Howard A.W., Noyes R.W., et al. 2009, ApJ 707, 446
Bryan, M.L., 2016, ApJ 821:89
Cuntz, M., 2012, Int. J. Astrobiology 11.1: 15-23
Dalba, P.A., Kane, S.R., Li, Z., et al. 2021, AJ 162, 154
Danchi, W.C., 2005, Proc Int Astron Union 1.C200: 65-70
Diaz, R.F., Demangeon, R.J., Hebrard, G., et al. 2016, A&A A146, 17
Döllinger, M.P. and Hartmann, M. 2021, ApJS 256:10
Dotter ,A. 2016, ApJS 222, 8
Feng, Y.K., 2015, ApJ 800:22
Fischer, D.A., Marcy, G.W., Butler, R.P., et al. 2001, ApJ 551, 1107

Gaudi, B.S., Seager, S., Mennesson, B., et al. 2018, Nat. Astron. 2, 600
Gallet, F., 2019, EAS Publ. Ser. 82: 59-69
Gettel, S. et al., 2012, ApJ 756:53
Ghezzi, L., Cunha, K., Schuler, S.C., et al. 2010, ApJ 725, 721
Giguere, M.J., Fischer, D.A., Payne, M.J., et al. 2015, ApJ 799 89
Giguere, M.J., Fischer, D.A., Payne, M.J., et al. 2012, ApJ 744, 4
Hirakawa, H. et al., 2015, ApJ 806:5
Jenkins, J.S., Jones, H.R.A., Tuomi, M., et al. 2017, MNRAS 466, 443
Jiang, J.H., Zhai, A.J. Herman, J. et al. 2018, AJ 156, 26
Jiang, J.H. and Zhu, S., 2018, Res. Notes AAS 2 185
Johnson, J.A., Clanton, C., Howard, A.W., et al. 2011, ApJS 197, 26
Jones, M.I., 2015, A&A 573, A3
Jones, M.I., Wittenmyer, R., Aguilera-Gomez, C., et al. 2021, A&A 646, A131
Kaltenegger, L. 2017, Annu. Rev. Astron. Astrophys 55, 433
Kopparapu, R.K., et al., 2013, ApJ, 765:131
Li Z., Kane, S.R., Dalba, P.A., et al. 2022, AJ 164, 163
Lopez, B., 2005, Proc Int Astron Union 1.C200: 93-98
Luhn, J.K., 2019, ApJ 157:149
Minniti, D., Paul, B.R., Lopez-Morales, M., et al. 2009, ApJ 693, 1424
Naef, D., Mayor, M., Lo Curto, G., et al. 2010, A&A 523, A15
O'Toole, S.J., Butler, R.P., Tinney, C.G., et al. 2007, ApJ 660, 1636
Ramirez, R.M. and Kaltenegger, L., 2016, ApJ, 823:6
Reichert, K., Reffert, S., Stock, S., et al., 2019, A&A, 625, A22
Robinson, S.E., Laughlin, G., Vogt S.S., et al. 2007, ApJ 670, 1391
Saio, B., Ando, H., Kambe, E., et al., 2003, ApJL, 597, L157
Sato, B. et al., 2013, ApJ 762:9
Selsis, F., Kasting, J.F., Levrard, B., et al. 2007, A&A 476, 1373
Sparrman, V. Masters Thesis, Uppsala University, 2022. URL: http://uu.diva-portal.org/smash/get/diva2:1670802/FULLTEXT01.pdf
Sreenivas, K.R., Perdelwitz, V., Tal-Or, L., et al. 2022, A&A 660, A124
Valenti, J.A. Fisher, D., Marcy, G.W., et al. 2009, ApJ 702, 989
Villaver, E. et al., 2014, ApJ, 794, 3
Vogt, S.S., Marcy, G.W., Butler, R.P, et al. 2000, ApJ 539, 902
Vogt, S.S., Butler, R.P., Marcy, G.W., et al. 2002, ApJ 568, 352
Zahn, J.-P., 1977, A&A, 57, 383.